CAMERA CALIBRATION COMBINING IMAGES WITH TWO VANISHING POINTS

L. Grammatikopoulos[a], G. Karras[a], E. Petsa[b]

[a] Laboratory of Photogrammetry, Department of Surveying,
National Technical University of Athens (NTUA), GR-15780 Athens, Greece
[b] Department of Surveying, The Technological Educational Institute of Athens (TEI-A),
Ag. Spyridonos Str., GR-12210 Athens, Greece
E-mail: lazaros@central.ntua.gr, gkarras@central.ntua.gr, petsa@teiath.gr

KEY WORDS: Calibration, Geometry, Distortion, Bundle, Non-Metric

ABSTRACT

Single image calibration is a fundamental task in photogrammetry and computer vision. It is known that camera constant and principal point can be recovered using exclusively the vanishing points of three orthogonal directions. Yet, three reliable and well-distributed vanishing points are not always available. On the other hand, two vanishing points basically allow only estimation of the camera constant (assuming a known principal point location). Here, a camera calibration approach is presented, which exploits the existence of only two vanishing points on several independent images. Using the relation between two vanishing points of orthogonal directions and the camera parameters, the algorithm relies on direct geometric reasoning regarding the loci of the projection centres in the image system (actually a geometric interpretation of the constraint imposed by two orthogonal vanishing points on the 'image of the absolute conic'). Introducing point measurements on two sets of converging image lines as observations, the interior orientation parameters (including radial lens distortion) are estimated from a minimum of three images. Recovery of image aspect ratio is possible, too, at the expense of an additional image.

Apart from line directions in space, full camera calibration is here independent from any exterior metric information (known points, lengths, length ratios etc.). Besides, since the sole requirement is two vanishing points of orthogonal directions on several images, the imaged scenes may simply be planar. Furthermore, calibration with images of 2D objects and/or 'weak perspectives' of 3D objects is expected to be more precise than single image approaches using 3D objects. Finally, no feature correspondences among views are required here; hence, images of totally different objects can be used. In this sense, one may still refer to a 'single-image' approach. The implemented algorithm has been successfully evaluated with simulated and real data, and its results have been compared to photogrammetric bundle adjustment and plane-based calibration.

1. INTRODUCTION

Recovering camera interior orientation is a basic task in photogrammetry and computer vision. Camera calibration approaches are generally classified into several categories, depending upon the prior knowledge of the recorded scene (known or unknown object geometry) and the type of the calibration objects, namely 3D object, plane pattern or 1D object (see Zhang, 2000; Gurdjos et al., 2002; Gurdjos & Sturm, 2003). Approaches, on the other hand, exploiting the existence of vanishing points have been reported in photogrammetry (Gracie, 1968; Bräuer-Burchardt & Voss, 2001; v. d. Heuvel, 2001; Grammatikopoulos et al., 2003) as well as in computer vision (Caprile & Torre, 1990; Liebowitz et al., 1999; Cipolla et al., 1999; Sturm & Maybank, 1999). This type of approach in fact exploits parallelism and perpendicularity among object primitives, commonly present in a man-made environment, for calibration and reconstruction purposes.

Indeed, it is known that the primary elements of interior orientation (camera constant, principal point location) can be recovered – along with the camera rotation matrix – using three orthogonal vanishing points on an image, whereby the principal point is the orthocentre of the triangle formed by the three vanishing points (Merritt, 1958; Gracie, 1968). Results have been reported in this context by Karras & Petsa (1999) and Bräuer-Burchardt & Voss (2001) for historic images (using known length ratios, the latter authors also address cases where one vanishing point is close to infinity). To the same effect, v. d. Heuvel (2001) adjusted line observations with constraints among lines for camera calibration. Relying on Petsa & Patias (1994), the authors have recently reported and assessed a formulation which combines in a single step the processes of line fitting, camera calibration (including radial lens distortion) and estimation of image attitude (Grammatikopoulos et al. 2003). Alternatively, in the context of

computer vision, several researchers perform camera calibration using three vanishing points in orthogonal directions, in order to compute the image ω of the absolute conic, and to subsequently decompose its expression to extract the camera internal parameters as the 'calibration matrix' (Liebowitz et al., 1999; Sturm & Maybank, 1999); the same outcome can be obtained by exploiting the properties of the rotation matrix (Cipolla et al., 1999). Despite the different conceptual framework, however, it can be proved that these above approaches are essentially equivalent to the analytical photogrammetric scheme of Gracie (1968).

But the existence on an image of three vanishing points suitable for reliable camera calibration (accurately recoverable and well distributed, i.e. none close to infinity) is admittedly not a trivial demand; pairs of vanishing points are considerably easier to obtain. Unless additional object constraints are imposed, however, this image type allows only to recover the camera constant with the hypothesis of known principal point location. Using historic photographs, Petsa et al. (1993) have rectified with this method façades of demolished buildings. Although, however, one single image with two vanishing points lacks the information for a full camera calibration, the combination of such images supplies the equations necessary for this task.

Thus, in this contribution a new camera calibration algorithm is developed, which exploits the existence of two vanishing points in orthogonal directions on several independent (single) images. Using the relation of these vanishing points to the camera parameters, the presented algorithm is based on a direct geometric interpretation regarding the locus of the projection centre in the image system. These loci are spheres, with centres belonging to the image plane and diameters fixed by the two orthogonal vanishing points. This non-linear equation involves explicitly the camera interior orientation parameters along with the four (in-

homogeneous) coordinates of the vanishing points. On the basis of this equation, simultaneous adjustment of observed points on lines imaged in each view allows to estimate the interior orientation elements of a 'normal' camera (camera constant, principal point) along with the radial symmetric lens distortion coefficients and, optionally, the image aspect ratio. Our approach presents certain similarities with that of Wilczkowiak et al. (2002), also a multi-view camera calibration approach not depending on image-to-image correspondences. A notable difference rests in the implicit involvement of vanishing points through the projection of parallelepipeds on the images, which apparently restricts the applications to scenes containing such primitives.

The presented algorithm has been successfully applied to both simulated and real data, and the outcome has been compared to a rigorous photogrammetric bundle adjustment and to plane-based calibration.

2. GEOMETRIC FORMULATION

2.1 The normal camera

As mentioned above, Gracie (1968) has given the six necessary equations relating the three interior orientation elements (camera constant, principal point) and image rotations (ω, φ, κ) to the vanishing points of three orthogonal directions. This is illustrated in Fig. 1, where O is the projection centre, c the camera constant and $P(x_o, y_o)$ the principal point, with V_X, V_Y, V_Z being the respective vanishing points of the three orthogonal space directions X, Y, Z. The principal point P, namely the projection of O onto the image plane, is actually the orthocentre of the triangle $V_X V_Y V_Z$. Of course, the directions of the lines OV_X, OV_Y, OV_Z are respectively parallel to the X, Y, Z space axes (and consequently they are mutually orthogonal).
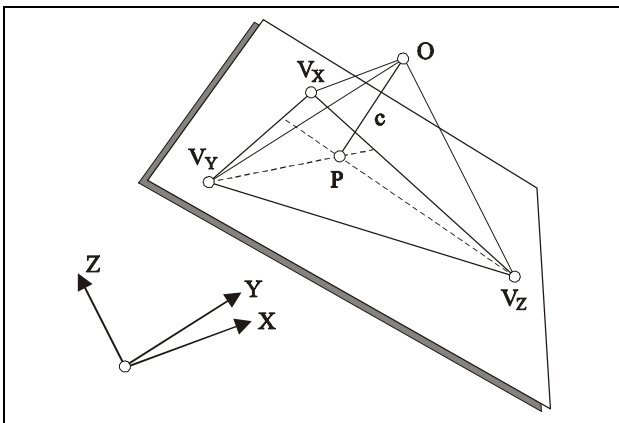

Figure 1. Image geometry with three vanishing points.

As mentioned already, in case two orthogonal vanishing points V_1, V_2 are known on the image plane while the third remains unknown, estimation of the interior orientation is feasible only if a fixed principal point can be assumed (usually the image centre). Hence, with only two vanishing points, the possible locations of the projection centre are obviously infinite. Yet, a constraint is always present: the image rays OV_1 and OV_2 form a right angle for all possible locations of O. This bounds the projection centre onto a geometrical locus, encompassing all points which see the two vanishing points under a right angle. Therefore, all possible locations of O in the 3D image space form a sphere (named here a 'calibration sphere') of radius R, with the middle M of line segment V_1V_2 as centre and the distance V_1V_2 as its diameter. Every point on this sphere represents a possible projection centre; the camera constant c equals then its distance from the image plane, while the principal point P is its projection onto it (see Fig. 2).
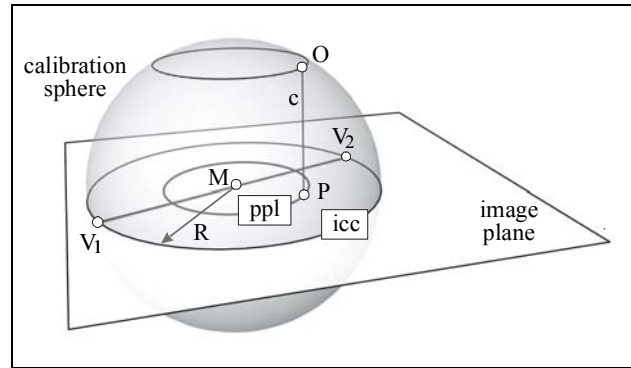

Figure 2. Calibration sphere as locus of the projection centre, principal point locus (ppl) and isocentre circle (icc)

The analytical equation of the sphere can be written as:

$$(x_o - x_m)^2 + (y_o - y_m)^2 + c^2 = R^2 \qquad (1)$$

with
$$x_m = \frac{x_1 + x_2}{2} \qquad y_m = \frac{y_1 + y_2}{2}$$

and
$$R = \frac{d}{2} = \frac{\sqrt{(x_1 - x_2)^2 + (y_1 - y_2)^2}}{2}$$

whereby (x_1, y_1), (x_2, y_2) are the two vanishing points, (x_m, y_m) is the centre of the sphere, R its radius and d its diameter. Every pair of orthogonal vanishing points gives one such Eq. (1). Two pairs of such vanishing points, from the same or from different images sharing identical internal parameters, define a circle (the intersection of the two spheres) as the locus for the projection centre, whereas a third pair – i.e. a third sphere – can fully calibrate the camera. In Fig. 3 the definition of the projection centre as intersection of three calibration spheres is illustrated. In actual fact, there exist two intersection points: 'above' and 'below' the image frame. This ambiguity is, of course, removed by keeping the point with c > 0 (point 'above' the image). In this sense one should speak of 'calibration semi-spheres' rather than spheres.
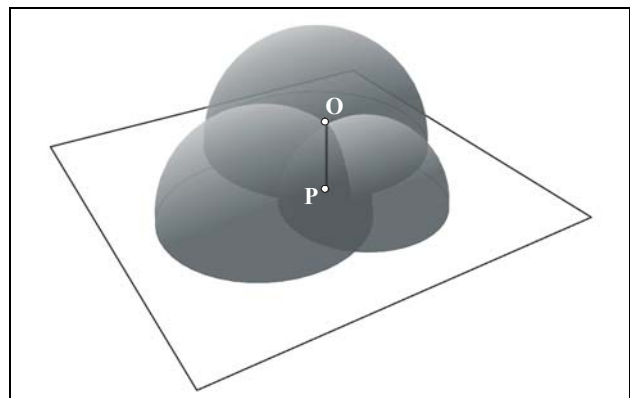

Figure 3. Projection centre O as intersection of three calibration spheres and principal point P as its projection on the image.

An equation equivalent to Eq. (1) is:

$$(x_o - x_m)^2 + (y_o - y_m)^2 = R^2 - c^2 \qquad (2)$$

which describes a circle on the image plane with centre (x_m, y_m) and the radius $(R^2 - c^2)^{1/2}$. This circle is the locus of the principal point P for a fixed camera constant c. In fact, as seen in Fig. 2, a fixed c constrains the projection centre on a circle of the sphere, which, being an intersection of the sphere with a plane parallel

to the image plane at a distance c from it, is also parallel to the image plane; when projected orthogonally onto it, the circle defines the principal point locus ('ppl' in Fig. 2).

On the other hand, it is worth mentioning that the circle formed as section of the sphere and the image plane itself (also seen in Fig. 2) is in fact the locus of the 'isocentre'. This image point – known in photogrammetric literature, thanks to its properties as regards measurement of angles on flat terrain (Church & Quinn, 1948) – lies on the bisector of the angle formed by the image rays to the principal point and to the third vanishing point (i.e. the vertical direction in the case of an oblique aerial image). Recently, Hartley & Silpa-Anan (2001) have used this point, as the 'conformal point', for measuring angles on the projected plane.

A further interesting geometrical aspect is that Eq. (1), after the substitutions, takes the following form:

$$(x_1 - x_o)x_2 + (y_1 - y_o)y_2 - x_o x_1 - y_o y_1 + x_o^2 + y_o^2 + c^2 = 0 \quad (3)$$

This equation represents the line (vanishing line), which passes through the second vanishing point $V_2(x_2, y_2)$, assuming that vanishing point V_1 and interior orientation parameters are known. Eq. (3) is the main equation of the calibration process to follow.

2.2 Consideration of the aspect ratio

All preceding equations and geometric interpretations hold for the case of a 'normal camera', whose only parameters are the camera constant and the principal point, under the assumption of square image pixels. Yet, there is the possibility of a non-square pixel, especially in CCD cameras. In these cases, introduction of an additional parameter is needed, namely of the camera aspect ratio a, which grasps the relative scaling of the two camera axes (for a normal camera $a = 1$). However, addition of this parameter does not change the basic geometric interpretation. Let $a < 1$ be the scale factor for the vertical (y) coordinates of the image points which, thus scaled, are the orthogonal projections of the initial 'normal' points onto an image plane, tilted by the angle β ($\cos β = a$) about the x-axis. The calibration sphere still holds for the normal plane but the projection of the 'isocentre circle' is an ellipse on the transformed (affine) image plane (see Fig. 4). The same is also true for the locus of the principal point (which, of course, coincides with the isocentre locus for c = 0).
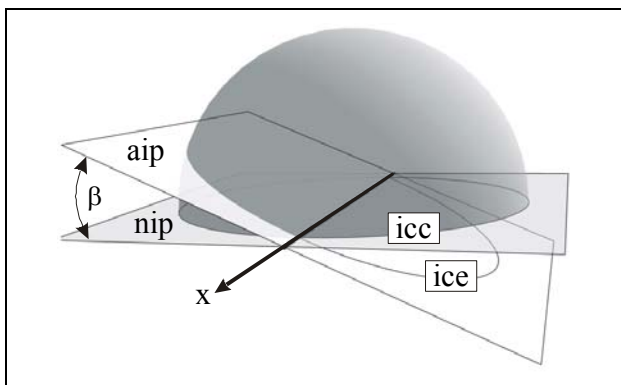

Figure 4. The isocentre ellipse (ice) is the orthogonal projection of the isocentre circle (icc) from the normal image plane (nip) onto the affine image plane (aip).The angle β between these two planes is related to the aspect ratio (a) as β = $\cos^{-1} a$.

Calibration equations Eq. (1) and Eq. (3) become, respectively:

$$(x_o - x_m)^2 + \left(\frac{1}{a^2}\right)(y_o - y_m)^2 + c^2 = R^2 \quad (4)$$

with

$$R = \frac{1}{2}\sqrt{(x_1 - x_2)^2 + \left(\frac{1}{a^2}\right)(y_1 - y_2)^2}$$

and

$$(x_1 - x_o)x_2 + \frac{(y_1 - y_o)y_2}{a^2} - x_o x_1 - \frac{y_o y_1}{a^2} + x_o^2 + \frac{y_o^2}{a^2} + c^2 = 0 \quad (5)$$

2.3 Calibration sphere and image of the absolute conic

As mentioned above, recovery of interior orientation is possible through an estimation of the image ω of the absolute conic from three orthogonal vanishing points (Liebowitz et al., 1999). The conic ω is defined as:

$$\omega = \mathbf{K}^{-T}\mathbf{K}^{-1} \quad (6)$$

where **K** is the calibration matrix (Hartley & Zisserman, 2000). Each pair of orthogonal vanishing points V_1, V_2 supplies a linear constraint on the entities of ω of the form

$$\mathbf{V}_1^T \omega \mathbf{V}_2 = 0 \quad (7)$$

whereby $\mathbf{V}_1$, $\mathbf{V}_2$ are in homogeneous representation. The two vanishing points are said to be conjugate with respect to ω. Three such pairs suffice for the estimation of the calibration matrix of a normal camera. Yet ω is an imaginary conic, and the geometric relation of the vanishing points with the camera internal parameters is not obvious. Ignoring aspect ratio (and skewness), ω may be written as:

$$\omega = \begin{bmatrix} 1 & 0 & -x_o \\ 0 & 1 & -y_o \\ -x_o & -y_o & x_o^2 + y_o^2 + c^2 \end{bmatrix} \quad (8)$$

Introducing Eq. (8) into (7), with $\mathbf{V}_1 = (x_1, y_1, 1)^T$, $\mathbf{V}_2 = (x_2, y_2, 1)^T$ in inhomogeneous representation, yields Eq. (1), the equation of the 'calibration sphere'. This means that constraint (7) and the sphere equation (1) are equivalent for inhomogeneous notation of vanishing points.

Next it will be seen that the calibration sphere is also relevant in the case of plane-based calibration, a process which estimates interior orientation using homographies **H** between a plane with known Euclidean structure and its images (Zhang, 2000). The two basic equations of plane-based calibration are:

$$\mathbf{h}_1^T \omega \mathbf{h}_2 = 0 \quad (9)$$

$$\mathbf{h}_1^T \omega \mathbf{h}_1 = \mathbf{h}_2^T \omega \mathbf{h}_2 \quad (10)$$

where $\mathbf{h}_1 = [H_{11}, H_{21}, H_{31}]^T$, $\mathbf{h}_2 = [H_{12}, H_{22}, H_{32}]^T$ are the first two columns of the **H** matrix. Each homography **H** provides two such constraints (9), (10) on the elements of ω. Gurdjos et al. (2002) put the problem of plane-based calibration into a more intuitive geometric framework, by proving that the solution is equivalent to intersecting circles ('centre circles'). The centre circle is the locus of the projection centre when space-to-image homography is known and can be obtained as intersection of a sphere (centre sphere) and a plane (centre plane). In photogrammetric terminology, this plane – typically defined in aerial images as the vertical plane containing the camera axis – is the 'principal plane'.

In fact, Eq. (9) is equivalent to the calibration sphere presented here. Using Eqs. (9) and (1), it is set:

$$D = \mathbf{h}_1^T \omega \mathbf{h}_2 = 0$$

$$G = (x_o - x_m)^2 + (y_o - y_m)^2 + c^2 - R^2 = 0$$

Taking into account that $\mathbf{V}_1 = [H_{11}, H_{21}, H_{31}]^T$, $\mathbf{V}_2 = [H_{12}, H_{22}, H_{32}]^T$ with respect to the elements of homography $\mathbf{H}$ and substituting them into G, it can be proved that G is equivalent to D only if $H_{31}H_{32} \neq 0$, which indicates that the first equation of plane-based calibration – Eq.(9) – is that of the calibration sphere when both vanishing points are finite.

3. THE CALIBRATION ALGORITHM

The developed calibration algorithm relies on the simultaneous estimation of two orthogonal vanishing points on each view, together with their common interior orientation elements. The vanishing points are estimated from individual point observations x_i, y_i on converging image lines. The fitted lines are constrained to converge to a corresponding vanishing point $V(x_V, y_V)$ according to following observation equation, whereby t represents the slope $\Delta x / \Delta y$ of the converging line with respect to the y axis:

$$x_i - x_V - (y_i - y_V)t = 0 \qquad (11)$$

According to each line direction, Eq. (11) is also formulated in terms of the slope $t = \Delta y / \Delta x$ with respect to the x-axis. Finally, introducing the coefficients k_1, k_2 of the radial symmetric lens distortion, Eq. (11) becomes (Gammatikopoulos et al., 2003):

$$x_i - (x_i - x_o)(k_1 r^2 + k_2 r^4) - x_V - \\ -\left[y_i - (y_i - y_o)(k_1 r^2 + k_2 r^4) - y_V\right]t = 0 \qquad (12)$$

The sum of squares of the image coordinate residuals are minimised in the adjustment. Alternative formulations of these equations are also possible, in order to minimise the distances of the points from the fitted line. Each individual point on a line of an image offers one such condition, (11) or (12), to the adjustment. Besides, every pair of vanishing points in orthogonal directions gives rise to one Eq. (1) or, equivalently, Eq. (3). It is clear that, if the normal camera is assumed, three pairs of vanishing points (i.e. images) suffice for an estimation of the internal camera parameters. The image aspect ratio a can also be integrated, at the expense of one additional pair of vanishing points (one image) using Eq. (4) or (5) instead of (1) or (3). All equations above are non-linear with respect to the unknowns, thus imposing a need for initial values. Generally, the principal point may be assumed at the image centre, the camera constant can then be approximated using a pair of vanishing points, line slope is estimated from two line points, while vanishing point coordinates can be approximated using two converging lines. Finally, it is worth noting that vanishing points might be weighted with the corresponding elements of the covariance matrix from a previous solution.

4. PRACTICAL EVALUATION

4.1 Synthetic data

For the practical evaluation of the algorithm both simulated and real data have been used. First, three sets consisting of 7, 13 and 22 synthetic images (1600×1200) of a 10×10 planar grid were generated with random exterior orientation (Fig. 5). All interior orientation parameters were kept invariant: c = 1600, x_o = 802, y_o = 604, $k_1 = 2×10^{-8}$, $k_2 = -3.5×10^{-14}$ (the aspect ratio has been ignored). Gaussian noise with zero mean and three standard deviations σ (±0.1, ±0.5, ±1 pixel) was added to the image points.
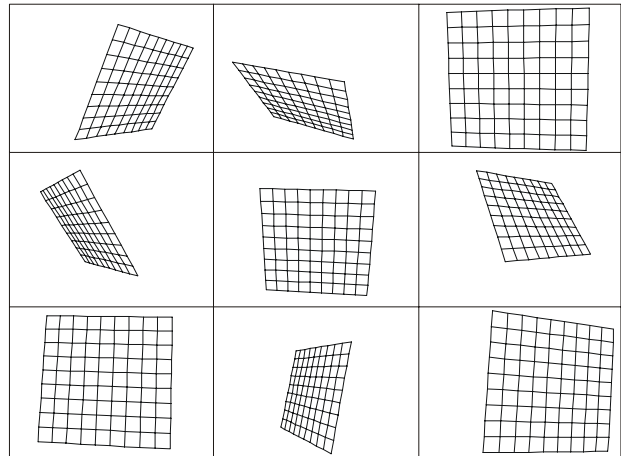

Figure 5. Some of the synthetic images used in the evaluation.

For all image sets, results were compared with plane-based calibration and self-calibrating bundle adjustment. Plane-based calibration was carried using the 'Calibration Toolbox for Matlab' of Bouguet (2004), available on the Internet (the latest version and complete documentation may be downloaded from the cited web site). The bundle adjustment – in which no tie points were used – has been carried out with the software 'Basta' (Kalisperakis & Tzakos, 2001). All results are presented in Tables 1–3.

Table 1. Results from 7 simulated images (noise: ±σ_N pixel)							
σ_N		Δc (‰)	Δx_o (pixel)	Δy_o (pixel)	k_1 (×10⁸)	k_2 (×10¹⁴)	σ_o (pixel)
0.1	CS	−0.26	−0.59	−0.20	1.95	−3.40	±0.10
	PB	0.15	0.01	0.02	1.96	−3.43	±0.10
	BA	0.20	−0.03	0.16	1.95	−3.43	±0.09
0.5	CS	1.42	1.39	−0.88	2.02	−3.66	±0.51
	PB	0.10	0.56	−0.08	1.99	−3.50	±0.50
	BA	0.08	0.55	−0.15	2.00	−3.49	±0.50
1.0	CS	1.99	−0.05	−2.90	1.93	−3.35	±0.99
	PB	1.62	−1.37	−2.58	1.70	−3.23	±0.99
	BA	1.54	−1.32	−2.42	1.70	−3.23	±1.00

Table 2. Results from 13 simulated images (noise: ±σ_N pixel)							
σ_N		Δc (‰)	Δx_o (pixel)	Δy_o (pixel)	k_1 (×10⁸)	k_2 (×10¹⁴)	σ_o (pixel)
0.1	CS	−0.28	−0.15	−0.13	2.03	−3.55	±0.10
	PB	−0.19	−0.05	−0.17	2.02	−3.54	±0.10
	BA	−0.18	−0.05	−0.11	2.02	−3.55	±0.10
0.5	CS	0.80	−2.90	−1.57	1.91	−3.37	±0.50
	PB	−0.62	−1.13	−0.93	1.80	−3.20	±0.49
	BA	−0.59	−1.23	−0.90	1.80	−3.20	±0.50
1.0	CS	1.49	−2.41	0.77	2.03	−3.46	±0.97
	PB	2.11	−0.98	1.22	1.78	−3.28	±0.97
	BA	2.13	−0.90	1.31	1.79	−3.29	±0.98

Table 3. Results from 22 simulated images (noise: ±σ_N pixel)							
σ_N		Δc (‰)	Δx_o (pixel)	Δy_o (pixel)	k_1 (×10⁸)	k_2 (×10¹⁴)	σ_o (pixel)
0.1	CS	0.15	0.02	0.12	1.99	−3.50	±0.10
	PB	0.11	−0.02	0.05	2.00	−3.50	±0.10
	BA	0.17	−0.04	0.08	2.00	−3.50	±0.10
0.5	CS	0.13	−1.43	−2.09	2.00	−3.50	±0.51
	PB	0.26	−0.64	−0.18	1.98	−3.49	±0.50
	BA	0.29	−0.74	−0.12	1.98	−3.49	±0.50
1.0	CS	1.20	−0.21	0.91	2.12	−3.56	±0.99
	PB	−0.56	0.20	0.81	2.04	−3.51	±0.97
	BA	−0.54	0.03	0.51	1.04	−3.51	±0.98

In the above Tables, c is given as deviation per mil, x_o and y_o as deviations in pixels, while k_1 and k_2 in true values. The symbols

CS, PB, BA stand, respectively, for calibration sphere, plane-based calibration and bundle adjustment. In all cases, the standard error of the unit weight (σ_o) is also given.

Generally, it is not quite possible to directly compare different results for the parameters of camera calibration, as in each case these are correlated to different quantities. Notwithstanding this fact, one could claim that the results of the developed algorithm compare indeed satisfactorily with both plane-based calibration and self-calibration, i.e. robust approaches resting on object-to-image correspondences (it is noted, however, that the latter two methods yield here almost identical results, basically due to object planarity and lack of tie points in self-calibration). Besides, only one set of noisy data has been introduced in each case, a fact implying that the presented results reflect the effects of the particular perturbations. Further tests are needed to establish the extent to which the method being studied is susceptible to noise.

4.2 Real data

For the application with real data, a set of 20 images (640×480) was used, drawn from the cited web site of Bouguet (Fig. 6). Calibration parameters were computed with all three methods. Table 4 presents the results for the parameters, along with their respective estimated precision; an exception is the aspect ratio, for which its deviation from unity ($1-a$) is presented. It must be noted that the specific plane-based algorithm used here does not explicitly compute the aspect ratio; besides, is uses a different model for radial distortion. Hence, these parameters have been transformed into the framework of the other two approaches.
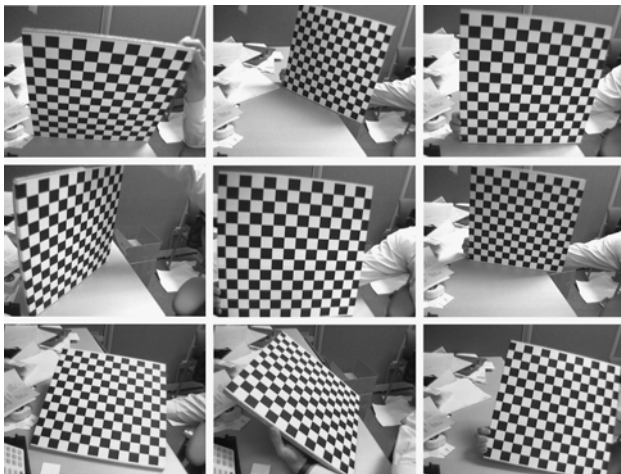

Figure 6. Nine of the images of Bouguet (2004) used here.

Table 4. Results for the data of Bouguet (20 images)							
	c (pixel)	$1-a$ (‰)	x_o (pixel)	y_o (pixel)	k_1 (×10^7)	k_2 (×10^{13})	σ_o (pixel)
CS	656.34 ±0.24	−2.8 ±0.3	302.34 ±0.12	242.09 ±0.23	−6.03 ±0.03	7.70 ±0.25	±0.12
PB	657.35 ±0.34	−0.6	302.92 ±0.56	242.98 ±0.60	−5.92	6.85	±0.13
BA	657.64 ±0.10	−0.6 ±0.1	301.48 ±0.17	239.79 ±0.15	−6.02 ±0.02	7.12 ±0.15	±0.09

Here again, it is seen that the results of the studied approach are essentially comparable to those of the other two methods. However, certain differences are evident (regarding the aspect ratio, for instance, or the camera constant); furthermore, the algorithm faced here a clear difficulty to converge. Actually, this problem was attributed to a particular image (seen at the far bottom right in Fig. 6). This particular view is characterised by a very weak perspective in one direction. Indeed, its rotation about the vertical Y axis is extremely small ($\phi = -0.58°$). The consequence is

that the vanishing point of the horizontal X direction tends to infinity (its x-coordinate is $x_{V_X} \approx 1.6 \times 10^5$). Although the algorithm proved to be indeed capable of handling even this unfavourable image geometry, exclusion of this particular image yielded the better results tabulated in the following Table 5.

Table 5. Results for the data of Bouguet (19 images)							
	c (pixel)	$1-a$ (‰)	x_o (pixel)	y_o (pixel)	k_1 (×10^7)	k_2 (×10^{13})	σ_o (pixel)
CS	657.49 ±0.27	−0.3 ±0.4	303.43 ±0.13	241.31 ±0.23	−6.05 ±0.03	7.86 ±0.27	±0.11
PB	657.29 ±0.34	−0.7	303.25 ±0.56	242.54 ±0.61	−5.94	7.01	±0.12
BA	657.59 ±0.10	−0.4 ±0.1	302.47 ±0.17	241.55 ±0.15	−6.03 ±0.02	7.18 ±0.17	±0.09

However, this example confirms that images with one (or both) of the vanishing points close to infinity might indeed undermine the adjustment. Having first estimated the initial values, a basic measure would be to automatically omit any image exhibiting a vanishing point (or a rotation ϕ or ω) which exceeds (or, respectively, is smaller than) a suitably selected threshold.

5. CONCLUDING REMARKS

Recently, the authors have reported on the photogrammetric exploitation of single uncalibrated images with one vanishing point for affine reconstruction (Grammatikopoulos et al., 2002), and on camera calibration using single images with three vanishing points (Grammatikopoulos et al., 2003). Here, a camera calibration algorithm is presented for independent single images with two vanishing points (in orthogonal directions). A direct geometric treatment has shown that, for such images, the loci of the projection centres in the image systems are (semi)spheres, each defined by the respective pair of vanishing points. The equation of this 'calibration sphere' relates explicitly the interior orientation parameters with the four (inhomogeneous) vanishing point coordinates. Actually, this is a – surely more familiar to photogrammetrists – geometric (Euclidean) interpretation of the projective geometry approaches adopted in computer vision.

Based on this, the implemented algorithm adjusts simultaneously all point observations on the two sets of concurring lines on each view. With ≥ 3 images, the outcome is estimations for camera constant, principal point location and radial lens distortion curve; for > 3 images, image aspect ratio can also be recovered. The algorithm has been tested with fictitious and real data. Although further experimentation is required, these first results indicate that – in terms of accuracy and precision – the presented method, which adjusts observations from all available images, compares very satisfactorily to both plane-based calibration and photogrammetric bundle adjustment.

This aspect needs to be underlined, since the latter two robust approaches are bound to space-to-image and/or image-to-image correspondences. The developed method, on the contrary, preserves all main advantages of a vanishing point based approach. Thus, there is no need for calibration objects or any prior metric information (points, lengths, analogies etc.). The mere existence of space lines in two orthogonal directions – a frequent appearance in a man-made environment – suffices for the calibration process. Evidently, this also implies that independent images (in principle, with identical interior orientation) of totally different 3D or planar scenes may well be used.

It is clear that an error analysis is needed to study the effects of the number of images as well as of the camera rotations relative to the space system axes (resulting in the position of the vanishing points on the image). The question of vanishing points tend-

ing to infinity must also be handled. Besides, the noise of image points has to be further investigated, with extensive tests using different noisy data and with real scenes.

A further future task would be to elaborate the approach into a semi-automatic or fully automatic process, by introducing tools for automatically detecting vanishing points (see, for instance, van den Heuvel, 1998; Rother, 2000). Finally, it is within the authors' intentions to extend the geometric model in order to incorporate the full calibration matrix (namely, to include image skewness) and, in addition, to accommodate the cases where the two vanishing points pertain to space directions which are not orthogonal to each other.

REFERENCES

Bräuer-Burchardt, C., Voss, K., 2001. Façade reconstruction of destroyed buildings using historical photographs. Proc. 19th CIPA Int. Symp., Potsdam, pp. 543-550.

Bouguet, J.-Y., 2004. Camera Calibration Toolbox for Matlab. http://www.vision.caltech.edu/bouguetj/calib_doc/

Caprile, B., Torre, V., 1990. Using vanishing points for camera calibration. Int. J. Comp. Vis., 4(2):. 127-140.

Church, E., Quinn, A.O., 1948. Elements of Photogrammetry. Syracuse Univ. Press, Syracuse, N.Y.

Cipolla, R., Drummond, T., Robertson, D.P., 1999. Camera calibration from vanishing points in images of architectural scenes. Proc. 10th BMVC, pp. 382-391.

Gracie, G., 1968. Analytical photogrammetry applied to single terrestrial photograph mensuration. XI ISP Congress, Lausanne.

Grammatikopoulos, L., Karras, G., Petsa, E., 2002. Geometric information from single uncalibrated images of roads. Int. Arch. Phot. Rem. Sens. 34(B5), pp. 21-26.

Grammatikopoulos, L., Karras, G., Petsa, E., 2003. Camera calibration approaches using single images of man-made objects. Proc. 19th CIPA Int. Symp., Antalya, pp. 328-332.

Gurdjos, P., Crouzil, A., Payrissat, R., 2002. Another way of looking at plane-based calibration: the centre circle constraint. Proc. ECCV '02, Springer, pp. 252-266.

Gurdjos, P., Sturm, P., 2003. Methods and geometry for plane-based self-calibration. Proc. CVPR '03, vol. 1, pp. 441-446.

Hartley, R., Zisserman, A., 2000. Multiple View Geometry in Computer Vision. Cambridge Univ. Press.

Hartley, R., Silpa-Anan, C., 2001. Visual navigation in a plane using the conformal point. Proc.10th Int. Symp. of Robotics Research, Lorne, Australia.

Kalisperakis, I., Tzakos, A., 2001. Bundle adjustment with self-calibration: program development and tests. Dipl. Thesis, Dept. of Surveying, NTUA.

Karras G., Petsa E., 1999. Metric information from single uncalibrated images. Proc. 17th CIPA Int. Symp., Olinda.

Liebowitz, D., Criminisi, A., Zisserman A., 1999. Creating architectural models from images. Eurographics '99, Computer Graphics Forum, 18(3), pp. 39-50.

Merritt, E. L., 1958. Analytical Photogrammetry. Pitman Publ. Co., New York.

Petsa, E., Karras, G., Aperghis, G., 1993. Zur Fassadenentzerrung aus Amateurbildern niedergerissener Altstadtviertel. Zeitschrift f. Vermessungswesen u. Raumordnung, 58(8):431-436.

Petsa E., Patias P., 1994. Formulation & assessment of straight-line based algorithms for digital photogrammetry. Int. Arch. Phot. Rem. Sens., 30(B5), pp. 310-317.

Rother C., 2000. A new approach for vanishing point detection in architectural environments. Proc. 11th BMVC, pp. 382–391.

Sturm, P., Maybank, S. J., 1999. A method for interactive 3D reconstruction of piecewise planar objects from single images. Proc. 10th BMVC, pp. 265-274

van den Heuvel, F.A., 2001. Reconstruction from a single architectural image from the Meydenbauer Archives. Proc. CIPA 18th Int. Symp., Potsdam, pp. 699-706.

van den Heuvel F., 1998. Vanishing point detection for architectural photogrammetry. Int. Arch. Phot. Rem. Sens., 32(B5), pp. 652-659

Wilczkowiak, M., Boyer, E., Sturm, P. F., 2002. 3D modeling using geometric constraints: a parallelepiped- based approach. Proc. ECCV '02, Springer, pp. 221-236.

Zhang Z., 2000. A flexible new technique for camera calibration. PAMI, 22(11), pp. 1330-1344.